

# Quasi Diabatic Propagation Scheme for Symmetric Quasi Classical Dynamics

Juan Sebastian Sandoval, Arkajit Mandal, and Pengfei Huo<sup>a)</sup>

Department of Chemistry, University of Rochester, 120 Trustee Road, Rochester, New York 14627, United States

We apply a recently developed quasi-diabatic (QD) scheme to the symmetric quasi-classical (SQC) approach for accurate quantum dynamics propagation. By using the adiabatic states as the quasi-diabatic states during a short-time quantum dynamics propagation, the QD scheme allows directly interfacing diabatic SQC method with commonly used adiabatic electronic structure calculations, thus alleviate tedious theoretical efforts to reformulate SQC in the adiabatic representation. Further, the QD scheme ensures a stable propagation of the dynamics and allows using a much larger time step compared to directly propagating SQC dynamics in the adiabatic representation. This is due to the fact that the QD scheme does not explicitly require non-adiabatic couplings that could exhibit highly peaked values during non-adiabatic dynamics propagation. We perform the QD-SQC calculations with a wide range of model non-adiabatic systems to demonstrate the accuracy of the proposed scheme. This study opens up the possibility for combining accurate diabatic quantum dynamics methods such as SQC with any adiabatic electronic structure calculations for non-adiabatic on-the-fly propagations.

## I. INTRODUCTION

The recently developed symmetric quasi-classical (SQC) approach<sup>1</sup> has shown great promise for providing accurate non-adiabatic dynamics.<sup>2–5</sup> By using the window function as the population estimator, SQC can significantly reduce the number of trajectories required for convergence,<sup>6</sup> while at the same time, recovers detailed balance with a reasonable accuracy<sup>7,8</sup> and provide a full description of the electronic density matrix.<sup>4,9</sup> New developments based on this scheme, such as coherence-controlled SQC<sup>10,11</sup> or extended SQC<sup>12</sup> have further improved the accuracy of this approach. That being said, SQC still faces some intrinsic deficiencies, such as inverted potential<sup>8</sup> that impact its numerical performance in recovering exact thermal equilibrium populations, or failed to achieve convergence for describing vibrational relaxation process.<sup>13</sup> Nevertheless, the quasi-classical nature of the SQC dynamics, together with many appealing features mentioned above makes it a promising method for simulating non-adiabatic on-the-fly dynamics of complex molecular systems.<sup>6</sup>

When performing on-the-fly simulations, the *adiabatic* representation is convenient for electronic structure calculations. Thus, the typical strategy for applying SQC (or other recently developed diabatic dynamics methods<sup>14–16</sup>) to “real” molecular systems is to reformulate them in the *adiabatic* representation,<sup>17</sup> which usually requires tedious theoretical efforts. Moreover, the adiabatic version of these methods are computationally inconvenient due to the presence of the first and second-order derivative couplings,<sup>17</sup> which could potentially lead to numerical instabilities during dynamical propagations.

Recently developed kinematic momentum (KM)-SQC approach<sup>17</sup> uses the *kinematic* momentum instead of the

canonical momentum as the dynamical variable, and explicitly eliminates the presence of the second-derivative coupling inside the equation of motion, thus significantly reducing the numerical cost. However this approach does require computing the time-dependent non-adiabatic coupling, therefore, it might encounter numerical instabilities when these couplings are highly peaked.

An alternative route is to employ *diabatic* electronic structure approaches<sup>18–22</sup> to perform on-the-fly simulations. Under this representation, the derivative couplings explicitly vanish, providing a more convenient representation for quantum dynamics propagation. However, these diabatic based approaches are not routinely available despite recent theoretical progress.<sup>18,19</sup>

To address this *discrepancy* between accurate *diabatic* quantum dynamics approaches and routinely available *adiabatic* electronic structure methods, we have developed a quasi-diabatic (QD) propagation scheme.<sup>23</sup> This scheme uses the adiabatic states as quasi-diabatic states during a short-time propagation, and dynamically update the QD states between two consecutive short-time propagations. It thus allows interfacing the routinely available *adiabatic* electronic structure calculations with accurate *diabatic* dynamics approaches.

In this work, we apply the QD propagation scheme<sup>23</sup> with the *diabatic* SQC approach for non-adiabatic dynamics simulations. We refer this approach as QD-SQC throughout this work. By using the QD scheme, we avoid any tedious effort to reformulate the diabatic SQC approach back into the adiabatic representation. Further, QD provides a much more stable propagation scheme by explicitly eliminating the presence of non-adiabatic couplings during dynamical propagation and thus allows using a much larger time step for propagation compared to the adiabatic SQC or KM-SQC. We demonstrate the accuracy and stability of QD-SQC propagation with a variety of non-adiabatic models. Throughout our model calculations, QD-SQC provides the exactly the same results as obtained from the diabatic SQC, with a similar time step for a stable dynamical propagation. This study

<sup>a)</sup> Electronic mail: pengfei.huo@rochester.edu

opens up the possibility for using QD-SQC to perform accurate on-the-fly non-adiabatic quantum dynamics for realistic and complex molecular systems.

## II. THEORY AND METHOD

### A. MMST Mapping Hamiltonian

We begin with a brief outline of the Meyer-Miller-Stock-Thoss mapping Hamiltonian,<sup>24–26</sup> which is one of the basic ingredients for many non-adiabatic dynamics approaches. The total Hamiltonian for a given molecular system can be expressed as a sum of the nuclear kinetic energy operator  $\hat{T}$  and the electronic Hamiltonian operator  $\hat{V}(\hat{\mathbf{r}}, \hat{\mathbf{R}})$  as follows

$$\hat{H} = \hat{T} + \hat{V}(\hat{\mathbf{r}}, \hat{\mathbf{R}}). \quad (1)$$

Here,  $\hat{\mathbf{r}}$  represents the coordinate operator of the electronic degrees of freedom (DOF), and  $\hat{\mathbf{R}}$  represents the coordinate operator of the nuclear DOF.

We start by expressing the total Hamiltonian in Eqn. 1 with strict *diabatic* basis  $\{|\alpha\rangle, |\beta\rangle\}$ , *i.e.*, a set of basis that does not explicitly depend on nuclear positions. With the diabatic basis, the total Hamiltonian is expressed as follows

$$\hat{H} = \hat{T} + \sum_{\alpha, \beta} V_{\alpha\beta}(\hat{\mathbf{R}}) |\alpha\rangle\langle\beta|, \quad (2)$$

where  $V_{\alpha\beta}(\hat{\mathbf{R}}) = \langle\alpha|\hat{V}(\hat{\mathbf{r}}, \hat{\mathbf{R}})|\beta\rangle$  is the state-dependent potential. By using the mapping representation of Meyer-Miller-Stock-Thoss<sup>24–26</sup> to transform the discrete electronic states into continuous variables, we have  $|\alpha\rangle\langle\beta| \rightarrow \hat{a}_\alpha^\dagger \hat{a}_\beta$ , where  $\hat{a}_\alpha^\dagger = (\hat{q}_\alpha - i\hat{p}_\alpha)/\sqrt{2}$  and  $\hat{a}_\beta = (\hat{q}_\beta + i\hat{p}_\beta)/\sqrt{2}$ . With this transformation, the original *diabatic* Hamiltonian is transformed into the following MMST mapping Hamiltonian

$$\hat{H}_m = \hat{T} + \frac{1}{2} \sum_{\alpha\beta} V_{\alpha\beta}(\hat{\mathbf{R}}) (\hat{p}_\alpha \hat{p}_\beta + \hat{q}_\alpha \hat{q}_\beta - 2\gamma \delta_{\alpha\beta}), \quad (3)$$

where  $\gamma = 0.5$  is the zero-point energy (ZPE) for the mapping harmonic oscillators (historically, it is recognized as the Langer correction by Meyer and Miller<sup>24</sup> for the quasi-classical description). Up to here, there is no approximation.

Instead of solving the equation of motion quantum mechanically, SQC assumes that the coupled electronic-nuclear dynamics is governed by the following Hamiltonian<sup>6</sup>

$$H_m = \frac{\mathbf{P}^2}{2M} + \frac{1}{2} \sum_{\alpha\beta} V_{\alpha\beta}(\mathbf{R}) (p_\alpha p_\beta + q_\alpha q_\beta - 2\gamma \delta_{\alpha\beta}). \quad (4)$$

Classical trajectories are generated based on the following Hamilton's equations of motion

$$\begin{aligned} \dot{q}_\alpha &= \partial H_m / \partial p_\alpha; \quad \dot{p}_\alpha = -\partial H_m / \partial q_\alpha \\ \dot{\mathbf{R}} &= \partial H_m / \partial \mathbf{P}; \quad \dot{\mathbf{P}} = -\partial H_m / \partial \mathbf{R} = \mathbf{F}, \end{aligned} \quad (5)$$

with the nuclear force expressed as

$$\mathbf{F} = -\frac{1}{2} \sum_{\alpha\beta} \nabla V_{\alpha\beta}(\mathbf{R}) (p_\alpha p_\beta + q_\alpha q_\beta - 2\gamma \delta_{\alpha\beta}). \quad (6)$$

Thus, MMST mapping Hamiltonian provides a consistent classical footing for both electronic and nuclear DOFs. The non-adiabatic transitions among electronic states are mapped onto the classical motion of fictitious harmonic oscillators.

### B. Symmetric Window Function Estimator

The equation of motion generated from  $\hat{H}_m$  (Eqn. 5) is equivalent to the Ehrenfest dynamics.<sup>14</sup> However, by using a window function<sup>1</sup> to restrain the initial mapping conditions and estimate the time-dependent population, SQC approach can significantly improve the numerical performance of non-adiabatic dynamics calculations, even with a Ehrenfest type equation of motion.

The SQC window function is formulated with the action-angle variables,  $\{n_\alpha, \theta_\alpha\}$ , which are related to the canonical mapping variables through the following relations

$$n_\alpha = \frac{1}{2} (p_\alpha^2 + q_\alpha^2 - 2\gamma); \quad \theta_\alpha = -\tan^{-1} \left( \frac{p_\alpha}{q_\alpha} \right), \quad (7)$$

and the inverse relations

$$q_\alpha = \sqrt{2(n_\alpha + \gamma)} \cos(\theta_\alpha); \quad p_\alpha = -\sqrt{2(n_\alpha + \gamma)} \sin(\theta_\alpha). \quad (8)$$

The SQC approach can be viewed as the classical Wigner model<sup>6</sup> resulted from linearized semi-classical approximations<sup>27</sup>, and calculates the population  $\rho_{\beta\beta}(t)$  with the initial density  $\hat{\rho}(0) = |\alpha\rangle\langle\alpha| \otimes \hat{\rho}_\mathbf{R}$  through the following expression

$$\begin{aligned} \rho_{\beta\beta}(t) &= \text{Tr}_\mathbf{R} \left[ \hat{\rho}_\mathbf{R} |\alpha\rangle\langle\alpha| e^{i\hat{H}t/\hbar} |\beta\rangle\langle\beta| e^{-i\hat{H}t/\hbar} \right] \\ &\approx \frac{1}{(2\pi\hbar)^{N+M}} \int d\boldsymbol{\tau} W_\mathbf{R}(\mathbf{P}, \mathbf{R}) W_\alpha(\mathbf{n}(0)) W_\beta(\mathbf{n}(t)). \end{aligned} \quad (9)$$

Here,  $W_\mathbf{R}(\mathbf{P}, \mathbf{R})$  is the Wigner density of  $\hat{\rho}_\mathbf{R}$  that contains  $M$  total nuclear DOF,  $\mathbf{n} = \{n_1, n_2, \dots, n_N\}$  is the action variable vector for  $N$  electronic states, with the corresponding angle variable vector  $\boldsymbol{\theta} = \{\theta_1, \theta_2, \dots, \theta_N\}$ , and  $d\boldsymbol{\tau} \equiv d\mathbf{P} d\mathbf{R} d\mathbf{n} d\boldsymbol{\theta}$ . Further,  $W_\alpha(\mathbf{n})$  is the Wigner transformed action variables<sup>9</sup>

$$W_\alpha(\mathbf{n}) = \delta(n_\alpha - 1) \prod_{\mu \neq \alpha} \delta(n_\mu), \quad (10)$$

The above results can be viewed as the Bohr-Sommerfeld quantization rule.<sup>9</sup>

In the SQC approach where the classical dynamics is used to solve Eqn. 5-6, the delta functions are better to be replaced by “pre-limit” delta functions, *i.e.*, the *window functions* that center at the integer values of the

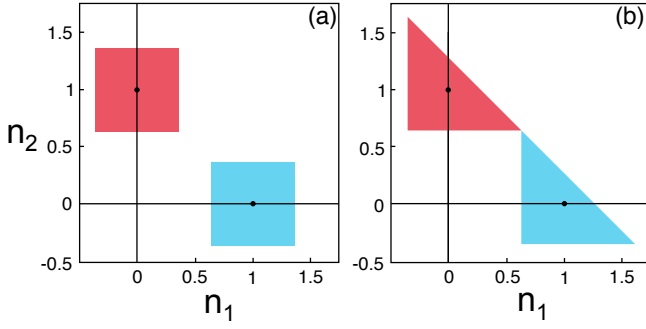


FIG. 1. Two possible choices for the window function in the action space: (a) square histogram windows with  $\gamma = \frac{1}{2}(\sqrt{3} - 1) \approx 0.366$  and (b) triangle histogram windows with  $\gamma = \frac{1}{3}$ . Here, the blue windows are used to estimate the population of state 1, and the red windows are used to estimate the population of state 2.

initial and final action variables, in order to facilitate the numerical convergence.<sup>6</sup> Further, in SQC approach,  $\gamma$  in Eqn. 4 is viewed as a parameter<sup>1,28</sup> instead of the ZPE of the mapping oscillator (with a value of 0.5).

Because these window functions are viewed as pre-limit delta function, *i.e.*, an approximation of Eqn. 11, they do not have a unique form,<sup>4</sup> and thus allowing the engineering aspect of the SQC approach. One can choose the following square window function<sup>1</sup>

$$W_\alpha(t) = w_1(n_\alpha) \prod_{\mu \neq \alpha} w_0(n_\mu), \quad (11)$$

where  $w_N$  is the square window function expressed as follows

$$w_n(n_\mu) = \frac{1}{2\gamma} h(\gamma - |n_\mu - n|). \quad (12)$$

Here,  $h(z)$  is the Heaviside function and  $n$  (either 0 or 1) is the electronic quantum number.

Fig. 1a depicts the above window function for a system with two electronic states, with the width  $\gamma = \frac{1}{2}(\sqrt{3} - 1) \approx 0.366$  suggested by Cotton and Miller.<sup>1</sup> Numerical results obtained from this window function have shown excellent agreement with the exact quantum dynamics for various model non-adiabatic systems.<sup>3,6</sup>

Fig. 1.b illustrates a recently proposed triangle window function.<sup>4</sup> For two-level systems, this triangle windowing function can be described with the following expression

$$W_1(t) = 2h(n_1 + \gamma - 1)h(n_2 + \gamma)h(2 - 2\gamma - n_1 - n_2) \quad (13)$$

$$W_2(t) = 2h(n_1 + \gamma)h(n_2 + \gamma - 1)h(2 - 2\gamma - n_1 - n_2),$$

with the width  $\gamma = \frac{1}{3}$ . This window function has shown a consistently better performance for two-level systems<sup>4,6</sup> compared to the square window function, as well as a more accurate description for the non-adiabatic transition rate over a broad range of electronic couplings.<sup>4</sup>

The time-dependent population at time  $t$  is then calculated by applying the window function estimator to actions variables  $\{n_\mu(t)\}$  for an ensemble of trajectories. Starting from the initial diabatic state  $|\alpha\rangle$ , the time-dependent population of the states  $|\beta\rangle$  is computed with Eqn. 9. However, by using the window function estimator, the total population is no longer properly normalized due to the fraction of trajectories that move out of any given window.<sup>1</sup> Thus, the population has to be normalized<sup>1</sup> with the following procedure

$$\rho_{\beta\beta}(t) / \sum_{\mu=1}^N \rho_{\mu\mu}(t) \rightarrow \rho_{\beta\beta}(t). \quad (14)$$

It should be noted that SQC is different compared to “Ehrenfest dynamics”, despite that they use the same equation of motion for the coupled electronic-nuclear DOFs.<sup>6,8</sup> The boundary conditions enforced by the window functions in SQC helps to eliminate several well-known deficiencies in Ehrenfest dynamics, such as the breakdown of detailed balance.<sup>7,8,29</sup>

Despite its simplicity, SQC has shown accurate description for non-adiabatic dynamics in a broad range of model systems.<sup>2-5</sup> It can also recover detailed balance with reasonable accuracy<sup>7,8</sup> and reach convergence with just a few thousand of trajectories.<sup>1,3,6</sup> It thus show great promise to accurately and efficiently perform *ab-initio* on-the-fly simulations for molecular systems.

### C. Quasi-Diabatic (QD) Propagation Scheme

For real molecular systems, strict diabatic states  $\{|\alpha\rangle\}$  are neither uniquely defined nor routinely available, despite recent theoretical progress.<sup>18-22</sup> Rather, it is convenient to solve the electronic structure problem under the *adiabatic* representation with the following eigenequation

$$\hat{V}(\hat{\mathbf{r}}, \mathbf{R})|\Phi_i(\mathbf{R})\rangle = E_i(\mathbf{R})|\Phi_i(\mathbf{R})\rangle. \quad (15)$$

Here,  $\hat{V}(\hat{\mathbf{r}}; \mathbf{R})$  is the electronic Hamiltonian operator defined in Eqn. 1 at a given nuclear configuration  $\mathbf{R}$ , and  $|\Phi_i(\mathbf{R})\rangle$  is the *adiabatic* state, *i.e.*, the eigenstate of  $\hat{V}(\hat{\mathbf{r}}; \mathbf{R})$ , with the corresponding eigenvalue  $E_i(\mathbf{R})$ . Most of the commonly used electronic structure methods are based on solving the above equation, providing eigenenergies and eigenfunctions under this representation.

The total Hamiltonian Eqn. 1, on the other hand, has a rather complicated expression (see Appendix A) under the *adiabatic* representation. This is due to the fact that adiabatic states are not the eigenfunctions of the nuclear kinetic energy operator  $\hat{T}$ . It is more convenient to develop new quantum dynamics methods in the strict diabatic representation (such as the diabatic SQC introduced in Sec. II A-II B). Thus, the typical strategy for applying new quantum dynamics approaches (like SQC) to “real” molecular systems is to reformulate them in the adiabatic representation.<sup>17</sup> However, this reformulating

process usually requires tedious theoretical efforts,<sup>14–17</sup> and the resulting adiabatic version of these methods are computationally inconvenient due to the presence of the first and second-order derivative couplings,<sup>17</sup> which could lead to numerical instabilities during dynamical propagations.

To address this discrepancy between accurate quantum dynamics methods in the diabatic representation and the electronic structure methods in the adiabatic representation, we have developed quasi-diabatic (QD) propagation scheme.<sup>23</sup> Here, we briefly summarize it by considering a short-time propagation of the nuclear DOF during  $t \in [t_1, t_2]$ , where the nuclear positions evolve from  $\mathbf{R}(t_1)$  to  $\mathbf{R}(t_2)$ , and the corresponding adiabatic states are  $\{|\Phi_i(\mathbf{R}(t_1))\rangle\}$  and  $\{|\Phi_k(\mathbf{R}(t_2))\rangle\}$ .

The essential idea of the QD scheme is to use the nuclear geometry at time  $t_1$  as the reference geometry,  $\mathbf{R}_0 \equiv \mathbf{R}(t_1)$ , and use the adiabatic basis  $\{|\Phi_i(\mathbf{R}(t_1))\rangle\}$  as the *quasi-diabatic* basis during this short-time quantum dynamics propagation, such that

$$|\Phi_i(\mathbf{R}_0)\rangle \equiv |\Phi_i(\mathbf{R}(t_1))\rangle, \text{ for } t \in [t_1, t_2]. \quad (16)$$

With the above QD basis (often called the “crude adiabatic basis”), the derivative couplings vanish in a trivial way, and  $\hat{V}(\hat{\mathbf{r}}; \mathbf{R})$  has off-diagonal elements. Because the electronic wavefunction changes rapidly with the motion of the nuclei, the QD basis is only convenient when the nuclear geometry  $\mathbf{R}$  is close to the reference geometry  $\mathbf{R}_0$ . Thus, during the next short-time propagation segment  $t \in [t_2, t_3]$ , we choose to use a new reference geometry  $\mathbf{R}'_0 \equiv \mathbf{R}(t_2)$  and *quasi-diabatic* basis  $|\Phi'_k(\mathbf{R}'_0)\rangle \equiv |\Phi_k(\mathbf{R}(t_2))\rangle$ .

We emphasize that there is always a non-removable part of the derivative coupling over the *entire configurational space* for polyatomic systems.<sup>30</sup> This is a well-known result in literature.<sup>18,19</sup> Here, the QD scheme circumvents this challenge by only requiring a set of *locally-defined diabatic* states, such that the derivative couplings vanish within the *configurational subspace* during a given short-time propagation.

Compared to the adiabatic representation, the advantage of the QD basis is that all of the derivative couplings vanish. As a consequence, the total Hamiltonian operator and the corresponding quantum dynamics propagation adapt a simpler form in the QD representation. With the nuclear geometry close to the reference geometry in each step, the QD states remains to be a convenient and compact basis in each short-term propagation segment. In addition, because of the diabatic nature of the QD basis, one can use any diabatic based approach to propagate the quantum dynamics. These approaches usually require diabatic energies, electronic couplings, and nuclear gradients. Between  $[t_1, t_2]$  propagation and  $[t_2, t_3]$  propagation segments, all of these quantities will be transformed from  $\{|\Phi_i(\mathbf{R}_0)\rangle\}$  basis to  $\{|\Phi'_k(\mathbf{R}'_0)\rangle\}$  basis.

With the above idea in mind, it is straightforward to obtain electronic couplings and nuclear gradients in the QD basis. During the  $t \in [t_1, t_2]$  short-time propagation,

the electronic Hamiltonian operator  $\hat{V}(\hat{\mathbf{r}}; \mathbf{R}(t))$  is evaluated under the QD states as

$$V_{ij}(\mathbf{R}(t)) = \langle \Phi_i(\mathbf{R}_0) | \hat{V}(\hat{\mathbf{r}}; \mathbf{R}(t)) | \Phi_j(\mathbf{R}_0) \rangle. \quad (17)$$

In practical on-the-fly calculations, the above quantity can be obtained from a linear interpolation between  $V_{ij}(\mathbf{R}(t_1))$  and  $V_{ij}(\mathbf{R}(t_2))$  as follows<sup>31</sup>

$$V_{ij}(\mathbf{R}(t)) = V_{ij}(\mathbf{R}(t_1)) + \frac{(t - t_1)}{(t_2 - t_1)} \left[ V_{ij}(\mathbf{R}(t_2)) - V_{ij}(\mathbf{R}(t_1)) \right]. \quad (18)$$

Here, the matrix elements  $V_{ij}(\mathbf{R}(t_1)) = \langle \Phi_i(\mathbf{R}_0) | \hat{V}(\hat{\mathbf{r}}; \mathbf{R}(t_1)) | \Phi_j(\mathbf{R}_0) \rangle = E_j(\mathbf{R}(t_1))\delta_{ij}$ , and the matrix elements  $V_{ij}(\mathbf{R}(t_2))$  can be easily computed as follows

$$V_{ij}(\mathbf{R}(t_2)) = \sum_{kl} b_{ik} \langle \Phi_k(\mathbf{R}(t_2)) | \hat{V}(\hat{\mathbf{r}}; \mathbf{R}(t_2)) | \Phi_l(\mathbf{R}(t_2)) \rangle b_{jl}^\dagger, \quad (19)$$

where  $\langle \Phi_k(\mathbf{R}(t_2)) | \hat{V}(\hat{\mathbf{r}}; \mathbf{R}(t_2)) | \Phi_l(\mathbf{R}(t_2)) \rangle = E_l(\mathbf{R}(t_2))\delta_{kl}$ ,  $b_{ik} = \langle \Phi_i(\mathbf{R}_0) | \Phi_k(\mathbf{R}(t_2)) \rangle$ , and  $b_{jl}^\dagger = \langle \Phi_l(\mathbf{R}(t_2)) | \Phi_j(\mathbf{R}_0) \rangle$ .

Similarly, the nuclear gradients on electronic Hamiltonian matrix elements  $\nabla V_{ij}(\mathbf{R}(t_2)) \equiv \partial V_{ij}(\mathbf{R}(t_2)) / \partial \mathbf{R}$  are evaluated as

$$\begin{aligned} \nabla V_{ij}(\mathbf{R}(t_2)) &= \nabla \langle \Phi_i(\mathbf{R}_0) | \hat{V}(\hat{\mathbf{r}}; \mathbf{R}(t_2)) | \Phi_j(\mathbf{R}_0) \rangle \quad (20) \\ &= \langle \Phi_i(\mathbf{R}_0) | \nabla \hat{V}(\hat{\mathbf{r}}; \mathbf{R}(t_2)) | \Phi_j(\mathbf{R}_0) \rangle \\ &= \sum_{kl} b_{ik} \langle \Phi_k(\mathbf{R}(t_2)) | \nabla \hat{V}(\hat{\mathbf{r}}; \mathbf{R}(t_2)) | \Phi_l(\mathbf{R}(t_2)) \rangle b_{jl}^\dagger. \end{aligned}$$

Here, we have used the fact that  $\{|\Phi_i(\mathbf{R}_0)\rangle\}$  is a *diabatic* basis during the  $[t_1, t_2]$  propagation, which allows moving the gradient operator to bypass  $\langle \Phi_i(\mathbf{R}_0) |$ . Moreover, we have inserted the resolution of identity  $\sum_k |\Phi_k(\mathbf{R}(t_2))\rangle \langle \Phi_k(\mathbf{R}(t_2))| = \mathbb{1}$ , where we explicitly assume that the QD basis at nuclear position  $\mathbf{R}(t_2)$  is complete. In a real molecular system, however, the basis at nuclear position  $\mathbf{R}(t_2)$  may not be a complete basis. As a consequence, the total population will decay from unity during the dynamical propagation. This problem can be easily addressed by performing orthonormalization procedure<sup>23</sup> among vectors  $\{|\Phi(\mathbf{R}(t_1))\rangle | \Phi_k(\mathbf{R}(t_2))\rangle\}$ .

Fig. 2 presents a simple two-level model system in panel (a) and its time-dependent electronic potential in the (b) diabatic, (c) adiabatic, and (d) quasi-diabatic representation. In Fig. 2a, the motion of the nuclear trajectory (indicated by the gray double-sided arrow) is confined on the diabatic state 1 (red surface). The diabatic potential energy surfaces  $V_{11}(R(t))$  and  $V_{22}(R(t))$  presented in panel (b) evolve smoothly in time, and the diabatic electronic coupling  $V_{12}$  is a small constant in this model. In panel (c), under the adiabatic representation, the derivative coupling vector  $d_{12}(R) = \langle \Phi_1(R) | \nabla \Phi_2(R) \rangle$  starts to exhibit large peaks at the avoided crossing regions, where the adiabatic wavefunctions rapidly change their characters. These rapid changes of derivative couplings usually cause numerical challenges and require a

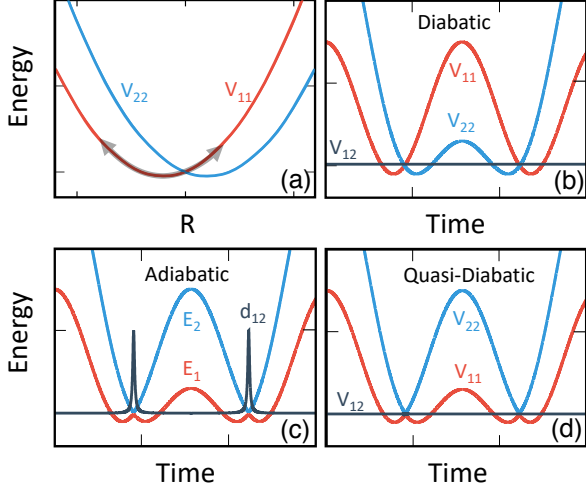


FIG. 2. (a) Diabatic potentials and the corresponding time-dependent potentials and couplings for a one-dimensional model system, in (b) diabatic representation, (c) adiabatic representation, and (d) quasi-diabatic representation.

very small time step for a stable quantum dynamics propagation. The QD representation presented in panel (d), on the other hand, vanishes the derivative couplings; the non-adiabatic transitions are induced by the overlap between two consecutive QD bases  $\langle \Phi_1(R(t_2)) | \Phi_2(R(t_1)) \rangle$ . The off-diagonal electronic coupling  $V_{12}(R(t))$  under QD has small values due to the varying QD basis along the propagation (see Eqn. 18), and will decrease to zero under the limit that  $(t_2 - t_1) \rightarrow 0$ .

Thus, the QD representation provides several unique advantages over the strict diabatic or adiabatic representation for quantum dynamics propagations. On one hand, the QD basis are constructed from the crude adiabatic basis, which can be easily obtained from any commonly used electronic structure calculations. On the other hand, the diabatic nature of the QD basis makes derivative couplings explicitly vanish and allows using any diabatic dynamics approaches to perform on-the-fly propagation. Further, the QD scheme ensures a stable propagation of the quantum dynamics compared to directly solving it in the adiabatic representation. This is due to the fact that directly solving electronic dynamics in the adiabatic state requires the non-adiabatic coupling  $\langle \Phi_j(\mathbf{R}(t)) | \frac{\partial}{\partial t} \Phi_i(\mathbf{R}(t)) \rangle = \mathbf{d}_{ji}(\mathbf{R}) \dot{\mathbf{R}}$ , which might exhibit highly peaked values and cause large numerical errors<sup>32,33</sup> when using the linear interpolation scheme.<sup>34</sup> The QD scheme explicitly alleviates this difficulty by using the well behaved transformation matrix elements  $\langle \Phi_j(\mathbf{R}(t_1)) | \Phi_i(\mathbf{R}(t_2)) \rangle$  instead of  $\langle \Phi_j(\mathbf{R}(t)) | \frac{\partial}{\partial t} \Phi_i(\mathbf{R}(t)) \rangle$ .

Further, we note that the QD scheme was historically introduced for propagating the electronic amplitudes in surface hopping calculations.<sup>31,35–37</sup> Recently, it has also been used in Gaussian wave packet dynamics approaches<sup>38–42</sup> and is referred as the moving crude adiabatic scheme.<sup>42</sup> Here, we significantly expand the scope

of this scheme<sup>23</sup> by using it as a general framework to interface any *diabatic* trajectory-based dynamics methods with any *adiabatic* electronic structure calculations.

#### D. Algorithm for QD-SQC propagation

Combining the diabatic SQC approach and the QD propagation scheme described above, we formulate the following algorithm for the QD-SQC quantum dynamics propagation:

1. sample the initial conditions of the nuclear DOF  $\mathbf{R}(t_1)$  and  $\mathbf{P}(t_1 + \frac{\Delta t}{2})$  based on the Wigner distribution  $W_{\mathbf{R}}(\mathbf{R}, \mathbf{P})$ ; uniformly sample the mapping action based on the window function  $W_{\mu}(\mathbf{n})$ , and the mapping angle variables  $\theta_{\mu} \in [0, 2\pi]$  for all electronic states  $|\mu\rangle$ .
2. perform electronic structure calculations at  $t_1$  to obtain the QD basis  $|\Phi_i(\mathbf{R}_0)\rangle \equiv |\Phi_i(\mathbf{R}(t_1))\rangle$ .
3. propagate nuclear positions as  $\mathbf{R}(t_2) = \mathbf{R}(t_1) + \mathbf{P}(t_1 + \frac{\Delta t}{2})\Delta t/M$ , perform electronic structure calculations at  $\mathbf{R}(t_2)$  to obtain the adiabatic basis  $\{|\Phi_k(\mathbf{R}(t_2))\rangle\}$ .
4. compute the electronic Hamiltonian elements  $V_{ij}(\mathbf{R}(t))$  based on Eqn. 18 for  $t \in [t_1, t_2]$ , as well as the nuclear gradients  $\nabla V_{ij}(\mathbf{R}(t_2))$  based on Eqn. 20.
5. propagate the canonical mapping variables  $\{\mathbf{q}, \mathbf{p}\}$  by solving Eqn. 5 with the electronic elements  $V_{ij}(\mathbf{R}(t))$  computed from step 4; propagate the nuclear momenta as  $\mathbf{P}(t_2 + \frac{\Delta t}{2}) = \mathbf{P}(t_1 + \frac{\Delta t}{2}) + \mathbf{F}(\mathbf{R}(t_2))\Delta t/M$ , with the force computed at nuclear position  $\mathbf{R}(t_2)$  based on Eqn. 6.
6. transform the canonical mapping variables from the instantaneous QD basis  $\{q_i, p_i\}$  back to the strict diabatic basis  $\{q_{\mu}, p_{\mu}\}$ , with  $q_{\mu} = \sum_i \langle \Phi_i(\mathbf{R}_0) | \mu \rangle q_i$  and  $p_{\mu} = \sum_i \langle \Phi_i(\mathbf{R}_0) | \mu \rangle p_i$ ; compute the action variables based on  $n_{\mu} = \frac{1}{2}(p_{\mu}^2 + q_{\mu}^2 - 2\gamma)$ ; evaluate the strict diabatic populations with the Window function estimator in Eqn. 11 or Eqn. 13, and renormalize population based on Eqn. 14.
7. transform the mapping variables into the new QD basis  $|\Phi'_k(\mathbf{R}_0)\rangle \equiv |\Phi_k(\mathbf{R}(t_2))\rangle$  for the  $[t_2, t_3]$  propagation step, with the following expressions:  $\sum_i q_i \langle \Phi_i(\mathbf{R}(t_1)) | \Phi_k(\mathbf{R}(t_2)) \rangle \rightarrow q_k$  and  $\sum_i p_i \langle \Phi_i(\mathbf{R}(t_1)) | \Phi_k(\mathbf{R}(t_2)) \rangle \rightarrow p_k$ .
8. repeat steps 3-7.

Here, we want to comment on three technical details for the QD propagation scheme. First, we have transformed the mapping variables between two bases in step 6 and 7. This process is valid because the relation between two QD bases in step 7 are  $|\Phi_k(\mathbf{R}(t_2))\rangle = \sum_i \langle \Phi_i(\mathbf{R}(t_1)) | \Phi_k(\mathbf{R}(t_2)) \rangle |\Phi_i(\mathbf{R}(t_1))\rangle$ . Since the mapping relation between the physical state and the singly excited oscillator state is  $|\Phi_k(\mathbf{R}(t_2))\rangle = a_k^{\dagger}|0\rangle = \frac{1}{\sqrt{2}}(\hat{q}_k + i\hat{p}_k)|0\rangle$ , the relations for the mapping variables associated

with two bases are

$$\begin{aligned} |\Phi_k(\mathbf{R}(t_2))\rangle &= \frac{1}{\sqrt{2}}(\hat{q}_k + i\hat{p}_k)|0\rangle \\ &= \sum_i \langle \Phi_i(\mathbf{R}(t_1)) | \Phi_k(\mathbf{R}(t_2)) \rangle \frac{1}{\sqrt{2}}(\hat{q}_i + i\hat{p}_i)|0\rangle. \end{aligned} \quad (21)$$

For molecular systems, one can always find a suitable choice for the basis set in order to make  $\langle \Phi_i(\mathbf{R}(t_1)) | \Phi_k(\mathbf{R}(t_2)) \rangle$  real, which guarantees that the mapping variables are transformed with the same relations as the bases. Similarly, in step 6, we transform the time-dependent mapping variables from the instantaneous QD basis,  $\{q_i, p_i\}$ , to the strict diabatic basis,  $\{q_\alpha, p_\alpha\}$ . Note that the relation between the strict diabatic  $\{|\alpha\rangle\}$  and QD  $\{|\Phi_i(\mathbf{r}; \mathbf{R}_0)\rangle\}$  states are  $|\alpha\rangle = \sum_i |\Phi_i(\mathbf{R}_0)\rangle \langle \Phi_i(\mathbf{R}_0) | \alpha \rangle$ , which leads to the following transformations for mapping variables associated with two bases

$$q_\alpha = \sum_i \langle \Phi_i(\mathbf{R}_0) | \alpha \rangle q_i; \quad p_\alpha = \sum_i \langle \Phi_i(\mathbf{R}_0) | \alpha \rangle p_i. \quad (22)$$

Second, the nuclear force evaluated in the QD basis in step 5 has the same form of the nuclear force in the strict diabatic basis  $\{|\alpha\rangle, |\beta\rangle\}$ . This is valid based on the following analysis. Consider expanding the strict diabatic basis as the linear combination of QD basis, with  $|\alpha\rangle = \sum_i |\Phi_i(\mathbf{R}_0)\rangle \langle \Phi_i(\mathbf{R}_0) | \alpha \rangle = \sum_\alpha C_{i\alpha} |\Phi_i(\mathbf{R}_0)\rangle$ . This implies that  $q_\alpha = \sum_i C_{i\alpha} q_i$  and  $p_\alpha = \sum_i C_{i\alpha} p_i$ . Plugging in these two expressions into the nuclear force  $\mathbf{F} = -\frac{1}{2} \sum_{\alpha\beta} \nabla V_{\alpha\beta}(R) [p_\alpha p_\beta + q_\alpha q_\beta - 2\gamma\delta_{\alpha\beta}]$  in the diabatic representation, we obtain the nuclear forces in the QD representation as follows

$$\begin{aligned} \mathbf{F} &= -\frac{1}{2} \sum_{ij\alpha\beta} C_{i\alpha} \nabla V_{\alpha\beta}(R) C_{j\beta} [p_i p_j + q_i q_j - 2\gamma\delta_{\alpha\beta}] \\ &= -\frac{1}{2} \sum_{ij} \nabla V_{ij}(R) [p_i p_j + q_i q_j - 2\gamma\delta_{\alpha\beta}], \end{aligned} \quad (23)$$

which indeed has the nuclear force expression in the diabatic representation.

Third, in step 6 we evaluate the population with the window function defined in the strict diabatic basis  $\{|\alpha\rangle, |\beta\rangle\}$ , despite that the mapping trajectories are propagated in the quasi-diabatic basis (in QD-SQC). We note that in real molecular systems, the strict diabatic states are not easily obtained. Thus, one might have to compute the population with the window function defined in the QD states, which is equivalent to the instantaneous adiabatic states. We will explore the consequence of using such window functions in future investigations. The focus of this paper, on the other hand, is to demonstrate that when the populations are evaluated with the *same* diabatic window functions, the results obtained from QD-SQC propagations are exactly the same as those obtained from the diabatic SQC propagations. We would also like

to emphasize that the accuracy of QD-SQC will be limited by the accuracy of SQC itself, *i.e.*, the validity of using a window function as an approximate pre-limit delta function, as well as the Ehrenfest-type mean-field dynamics. The QD propagation scheme is rather general and provides a convenient framework that allows interfacing *diabatic* dynamics approaches with *adiabatic* electronic structure calculations for on-the-fly propagation.<sup>23</sup>

## E. Details of Model Calculations

**Electronic Matrix Elements for the QD propagation.** For model calculations in this paper, the matrix elements of the electronic Hamiltonian  $V_{\alpha\beta}(\mathbf{R}(t))$  and the nuclear gradients in the diabatic representation  $\nabla V_{\alpha\beta}(\mathbf{R}(t))$  are available and directly used in SQC propagations. For QD-SQC propagations, the adiabatic basis  $\{|\Phi_i(\mathbf{r}; \mathbf{R}(t))\rangle\}$  is obtained by diagonalizing  $V_{\alpha\beta}(\mathbf{R}(t))$  matrix, which is used as the QD basis. The matrix elements of the electronic Hamiltonian and nuclear gradients are evaluated using Eqn. 17-19 and Eqn. 20, respectively. Alternatively, these elements can be easily computed by taking advantage of the available diabatic basis in all of our model calculations, for example, as  $V_{ij}(\mathbf{R}(t)) = \sum_{\alpha\beta} \langle \Phi_i(\mathbf{R}_0) | \alpha \rangle V_{\alpha\beta}(\mathbf{R}(t)) \langle \beta | \Phi_j(\mathbf{R}_0) \rangle$ . Both protocols generate the same results.

**Initial Conditions.** The initial conditions for all of the model calculations are  $\hat{\rho}(0) = |\alpha\rangle\langle\alpha| \otimes \hat{\rho}_{\mathbf{R}}$ , where  $|\alpha\rangle$  indicates the initial electronic diabatic state and  $\hat{\rho}_{\mathbf{R}}$  represents the initial nuclear density operator. For non-adiabatic scattering and photo-dissociation calculations presented in Fig. 5-6, we use  $\hat{\rho}_{\mathbf{R}} = |\chi\rangle\langle\chi|$ , where  $\langle \mathbf{R} | \chi \rangle = \left(\frac{2\Gamma}{\pi}\right)^{1/4} e^{-(\Gamma/2)(\mathbf{R}-\mathbf{R}_0)^2 + \frac{i}{\hbar} \mathbf{P}_0(\mathbf{R}-\mathbf{R}_0)}$  represents a Gaussian wavepacket centered around  $\mathbf{R}_0$  and  $\mathbf{P}_0$  with a width  $\Gamma$ . The corresponding nuclear Wigner density is  $W_{\mathbf{R}}(\mathbf{P}, \mathbf{R}) = \frac{1}{\pi} e^{-\Gamma(\mathbf{R}-\mathbf{R}_0)^2 - (\mathbf{P}-\mathbf{P}_0)^2/\Gamma}$ . For the condensed-phase model calculations presented in Fig. 7-8, we assume that each nuclear DOF is represented by a harmonic mode. The canonical thermal density for the  $\nu_{\text{th}}$  nuclear DOF  $R_\nu$  is thus  $\hat{\rho}_{\mathbf{R}}(\hat{P}_\nu, \hat{R}_\nu) = \frac{1}{\mathcal{Z}} e^{-\frac{1}{\hbar^2} [\hat{P}_\nu^2/2M + \frac{1}{2} M \omega_\nu^2 \hat{R}_\nu^2]}$ . The corresponding nuclear Wigner density is then  $W_{\mathbf{R}}(P_\nu, R_\nu) = 2 \tanh\left(\frac{\omega_\nu}{2k_B T}\right) e^{-\tanh\left(\frac{\omega_\nu}{2k_B T}\right) [m\omega_\nu(R_\nu - R_\nu(0))^2 + P_\nu(0)^2/(m\omega_\nu)]}$ .

**Model Hamiltonians.** The spin-boson model has the Hamiltonian  $\hat{H} = \sum_\nu [\hat{P}_\nu^2/2 + \omega_\nu^2 \hat{R}_\nu^2/2 + c_\nu \hat{R}_\nu \hat{\sigma}_z] + \epsilon \hat{\sigma}_z/2 + \Delta \hat{\sigma}_x$ , with electronic bias  $\epsilon$ , electronic coupling  $\Delta$ , and the system-bath coupling  $c_\nu$  for a given spectral density  $J(\omega) = \frac{\pi}{2} \sum_\nu \frac{c_\nu^2}{\omega_\nu} \delta(\omega - \omega_\nu)$ . Here, we use 100 discretized harmonic modes to sample<sup>43</sup> the spectral density  $J(\omega) = \frac{\pi}{2} \xi \omega e^{-\omega/\omega_c}$ , where  $\xi$  is the Kondo parameter and  $\omega_c$  is the cut-off frequency (peak of the spectral density). For the model calculations in this paper, we use  $\Delta = 1$  and  $\omega_c = 2.5$  (Fig. 8a-c) or  $\omega_c = 1$  (Fig. 8d). The initial Wigner distribution for the bath modes is centered around  $R_\nu(0) = -c_\nu/\omega_\nu^2$  and  $P_\nu(0) = 0$ .

For simulating singlet excitation energy transfer in a



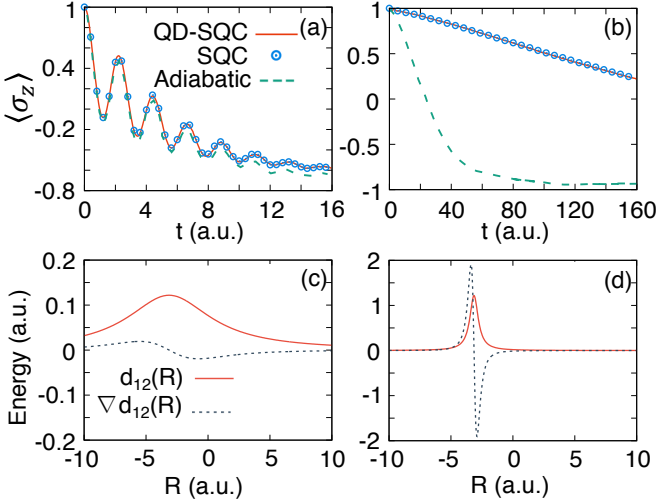


FIG. 3. Population dynamics of the spin-boson model in (a) strong (b) weak diabatic electronic coupling regime, obtained from SQC calculation in the diabatic (open circles), adiabatic (dash), and quasi-diabatic (solid) representation. In the adiabatic SQC calculation, the second derivative couplings are ignored.<sup>17</sup> Derivative coupling  $d_{12}(R)$  and its derivative  $\nabla d_{12}(R)$  are calculated for both scenarios and presented in panels (c) and (d). The  $R$  coordinate is chosen based on its frequency, which is closest to  $\omega_c$ .

dissipative environment, we use the following Frenkel exciton model  $\hat{H} = \hat{H}_e + \hat{H}_{ep}$ . The electronic part of the Hamiltonian is  $\hat{H}_e = \sum_{\alpha} \epsilon_{\alpha} |\alpha\rangle\langle\alpha| + \sum_{\alpha \neq \beta} \Delta_{\alpha\beta} |\alpha\rangle\langle\beta|$ , with singlet excitation energy  $\epsilon_{\alpha}$  on chromophore  $\alpha$  and the electronic coupling  $\Delta_{\alpha\beta}$  between two single excitations  $|\alpha\rangle$  and  $|\beta\rangle$ . The electron-phonon interaction Hamiltonian is  $\hat{H}_{ep} = \sum_{\alpha} \sum_{\nu_{\alpha}} [\frac{1}{2}(\hat{P}_{\nu_{\alpha}}^2 + \omega_{\nu_{\alpha}}^2 \hat{R}_{\nu_{\alpha}}^2) + c_{\nu_{\alpha}} \hat{R}_{\nu_{\alpha}} |\alpha\rangle\langle\alpha|]$ , where each state  $|\alpha\rangle$  is coupled to a set of independent harmonic bath modes  $\{R_{\nu_{\alpha}}\}$ . Here, we use the model parameters of the Fenna-Matthews-Olson (FMO) complex that contains seven chromophores.<sup>44</sup> In addition, we use 60 modes to sample the spectral density  $J(\omega) = 2\lambda\omega\tau/(1 + (\omega\tau)^2)$  for each bath, where the reorganization energy is  $\lambda = 35 \text{ cm}^{-1}$ , and the solvent response time is  $\tau = 50 \text{ fs}$ . The parameters for  $\hat{H}_e$  can be found in Ref. 44 and the sampling procedure in Ref. 3. The initial Wigner distribution for each bath mode is centered around  $\mathbf{R}(0) = 0$  and  $\mathbf{P}(0) = 0$ .

**Window Functions and Convergence.** In this paper, all of the calculations for two level systems are performed with the triangle window function (Eqn. 13), which has been shown to provide the accurate electronic dynamics across a broad range of the electronic couplings.<sup>4</sup> The only results obtained with square window function are the seven-states excitation energy transfer calculations<sup>44</sup> presented in Fig. 7. All of the results are obtained with 24,000 trajectories, except those in FMO model (Fig. 7) where 200,000 trajectories are used. The same time step  $dt$  are used for both SQC and QD-SQC calculations.

### III. RESULTS AND DISCUSSIONS

Fig. 3 presents the results of the spin-boson model. In these model calculations, the temperature is  $(k_B T)^{-1} = 5$ , the energy bias is  $\epsilon = 1$ , and the parameters for the bath are  $\omega_c = 2.5$  and  $\xi = 0.1$ . The diabatic electronic coupling is (a)  $\Delta = 1$  for the adiabatic regime (such that  $(k_B T)^{-1} \Delta \gg 1$ ) or (b)  $\Delta = 0.1$  for the non-adiabatic regime (such that  $(k_B T)^{-1} \Delta \ll 1$ ). The results are obtained from the original diabatic SQC (open circles), QD-SQC (solid lines), and the adiabatic SQC propagation<sup>17</sup> (dash lines), with the details of adiabatic mapping Hamiltonian provided in Appendix A. For the adiabatic SQC approach, the gradient of the derivative coupling term  $\nabla d_{12}(\mathbf{R})$  has been ignored in the dynamical propagation,<sup>17</sup> because they are equivalent to second-order derivative couplings and very expensive to obtain in regular electronic structure calculations.<sup>17</sup> It can be clearly seen that, while SQC and QD-SQC provide identical results (with the same numerical cost), the adiabatic SQC completely breakdown in the non-adiabatic regime presented in panel (b). This due to the fact that  $\nabla d_{12}(\mathbf{R})$  is much larger in the non-adiabatic regime (weak diabatic coupling regime) compared to the adiabatic regime (strong diabatic coupling regime). Fig.3c and 3d depict both the first derivative coupling term  $d_{12}(R)$  and its derivative  $\nabla d_{12}(R)$  for a particular nuclear mode  $R$  that has the closest frequency compared to  $\omega_c$ , with the corresponding electronic coupling in (a) and (b). One can clearly see that the derivative coupling  $d_{12}(R)$  exhibit large peaks and a rapidly change near the avoiding crossing regions, which is even more pronounced for  $\nabla d_{12}(R)$ , especially in the non-adiabatic regime. Thus, simply ignore it will cause large numerical error for dynamics,<sup>17</sup> especially when it is even larger than derivative coupling itself. Comparisons between the SQC-based approaches and the numerically exact results are also provided in Appendix C.

We should note that, with the recently developed KM-SQC approach<sup>17</sup> (with details provided in Appendix B), the kinematic momentum transform explicitly eliminates the presence of  $\nabla d_{12}(\mathbf{R})$  term in the nuclear force (instead of ignoring it), thus help achieving accurate results in the non-adiabatic regime presented in panel (b). However, KM-SQC explicitly contains the derivative couplings in the mapping equations (see Eqn. 29 in Appendix B). Thus, it might exhibit numerical challenge when derivative couplings are highly peaked and requires a much smaller time step for a stable propagation.

Fig. 4 presents the relative error of the action variable  $n_{\alpha} = \frac{1}{2} (p_{\alpha}^2 + q_{\alpha}^2 - 2\gamma)$  in a simple avoided crossing model (Tully's Model I) at a long time ( $t \rightarrow \infty$ ). This relative error is defined as  $P_{\text{error}} = [n_{\alpha}(dt) - n_{\alpha}(dt \rightarrow 0)]/n_{\alpha}(dt \rightarrow 0)$ , where  $n_{\alpha}(dt)$  is the action obtained with  $dt$  time step, and  $n_{\alpha}(dt \rightarrow 0)$  is the action obtained with a very small  $dt$ , such that the value of the action converges. The results are obtained from adiabatic-SQC (solid line), KM-SQC (open circle) and QD-SQC (solid

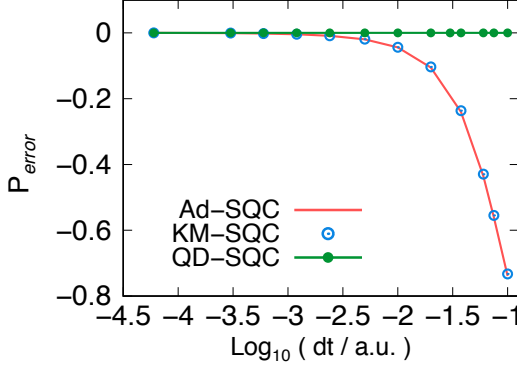


FIG. 4. The relative error of the action variable in a simple avoided crossing model (Tully’s Model I), obtained from adiabatic-SQC (solid line), KM-SQC (open circle) and QD-SQC (solid line with filled circles).

line with filled circles). This relative error is computed from a single SQC trajectory, with initial nuclear condition  $R_0 = -9.0$  a.u. and  $P_0 = 30$  a.u., and initial mapping condition  $n_1 = 1.0$ ,  $n_2 = 0.0$ , and  $\theta_1 = \theta_2 = \pi/4$ ; a consistent numerical behavior of this error with other initial conditions is observed. From this figure, it is clear that both KM-SQC and adiabatic-SQC require a much smaller time step to achieve converged results, due to the explicit presence of  $\langle \Phi_j(\mathbf{R}(t)) | \frac{\partial}{\partial t} \Phi_i(\mathbf{R}(t)) \rangle = \mathbf{d}_{ji}(\mathbf{R}) \dot{\mathbf{R}}$  in the equation of motion (see Eqn. 29 in Appendix B). QD-SQC, on the other hand, provides more accurate results even when a relatively larger time step is used, because it only requires the well behaved transformation matrix elements  $\langle \Phi_j(\mathbf{R}(t_1)) | \Phi_i(\mathbf{R}(t_2)) \rangle$ , instead of the highly peaked  $\langle \Phi_j(\mathbf{R}(t)) | \frac{\partial}{\partial t} \Phi_i(\mathbf{R}(t)) \rangle$  or  $\mathbf{d}_{ji}(\mathbf{R})$ .

Fig. 5 presents the results of Tully’s three non-adiabatic scattering models,<sup>45</sup> with (a) single avoided crossing (Tully’s Model I), (b) dual avoided crossing (Tully’s Model II), and (c) extended coupling with reflection (Tully’s Model III). These results are obtained from the diabatic SQC (open circles), QD-SQC (solid lines), and numerical exact split-operator Fourier transform method (dash lines). Initial nuclear conditions are sampled from the Wigner transformed Gaussian wavepacket, with  $\Gamma=1$  a.u.,  $R_0 = -9.0$  a.u., and  $P_0 = 30$  a.u. Fig. 5a-c provide the population  $\rho_{11}(t)$  (red) and  $\rho_{22}(t)$  (blue). QD-SQC gives the same results as those obtained from diabatic SQC; both are close to the numerical exact results. Fig. 5d presents the asymptotic diabatic population of Tully’s model II as a function of the center momenta  $P_0 = \hbar k$  for the initial nuclear wavepacket. Again, QD-SQC provides the same results as the diabatic SQC, and both are close to the numerical exact ones.

Fig. 6 presents the results for a two-state, three-mode conical intersection model.<sup>28,46</sup> Here, the three modes are indicated as  $R_\nu \in \{R_1, R_{6a}, R_{10a}\}$ , and the model Hamiltonian has the form  $\hat{H} = \sum_\nu \frac{1}{2} [P_\nu^2 + \omega_\nu^2 R_\nu^2] + \sum_\alpha [E_\alpha + \sum_\nu c_\nu^\alpha R_\nu] |\alpha\rangle\langle\alpha| + \lambda R_{10a} [|1\rangle\langle 2| + |2\rangle\langle 1|]$ . The parameters can be found in Ref. 28. Both the non-

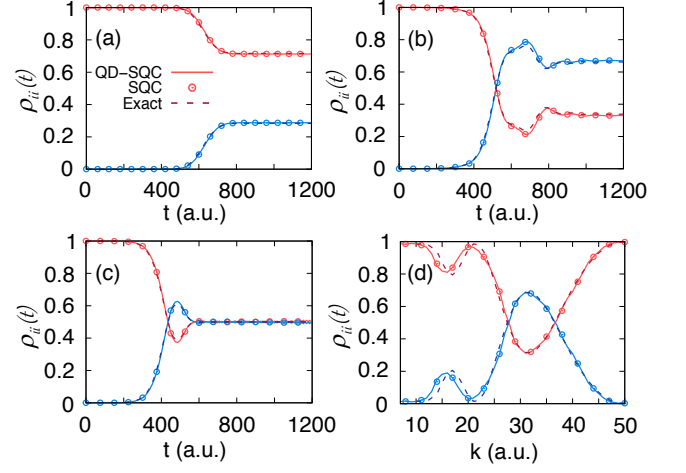


FIG. 5. Diabatic state population of Tully’s scattering models, with (a) Model I, (b) Model II, and (c) Model III. Results are obtained from SQC (open circles), QD-SQC (solid) and numerical exact calculations (dash). (d) Asymptotic diabatic population of model II as a function of various center momenta  $P_0 = \hbar k$  of the initial nuclear wavepacket.

adiabatic coupling element  $\langle \Phi_1(\mathbf{R}(t)) | \frac{\partial}{\partial t} \Phi_2(\mathbf{R}(t)) \rangle$  and the derivative coupling vector diverge near the conical intersection, creating numerical challenges for directly propagating dynamics in the adiabatic representation. The QD scheme avoids this challenge because it only requires  $\langle \Phi_1(\mathbf{R}(t_1)) | \Phi_2(\mathbf{R}(t_2)) \rangle$  for the basis transformation during the dynamical propagation. Fig. 6 demonstrates that QD-SQC exactly reproduces the diabatic SQC results, with (a) the diabatic population of state  $|2\rangle$  and (b)-(d) expectation values of the nuclear positions and momenta. In addition, both SQC and QD-SQC provide reasonably accurate results compared to the numerical exact ones.

Finally, Fig. 7 presents the quantum dynamics results for an excitation energy transfer (EET) model system.<sup>44</sup> Here, instead of using the triangle shaped window function, we use the original square shaped window function with a width  $\gamma = 0.336$ . The diabatic state population are obtained from the SQC (open circles), QD-SQC (solid lines), as well as exact results (dash lines) from hierarchy equations of motion (HEOM) approach.<sup>44</sup> Two different initial excitation are considered, with (a) state  $|1\rangle$  and (b) state  $|6\rangle$ . As can be clearly seen, QD-SQC exactly reproduces SQC results, which are reasonably accurate compared to the numerical exact results.

#### IV. CONCLUSIONS

We apply the recently developed quasi-diabatic (QD) scheme<sup>23</sup> to propagate quantum dynamics with symmetric quasi-classical (SQC) approach.<sup>1</sup> Using the instantaneous adiabatic states as the QD states during a short-time propagation, we can directly use the diabatic based



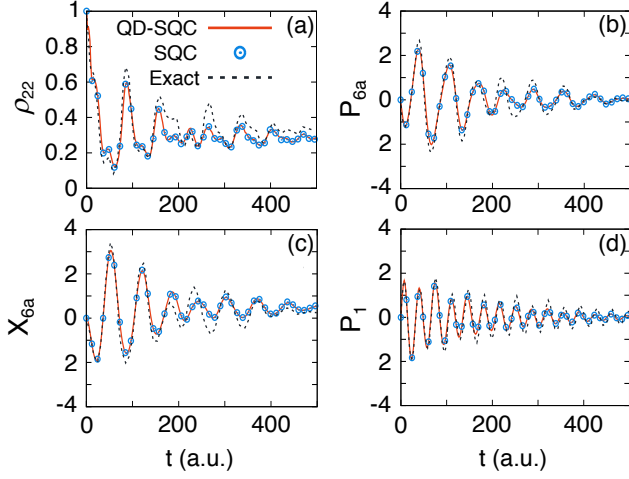


FIG. 6. Quantum dynamics in a conical intersection model of pyrazine, with (a) diabatic population of state  $|2\rangle$ , (b) average momentum of the  $6a$  mode, (c) average position of the  $6a$  mode and (d) average momentum of the symmetric mode. Results are obtained from SQC (open circles), QD-SQC (solid), and numerical exact calculations (dash).

SQC to propagate quantum dynamics, avoid any additional tedious efforts for redeveloping this approach in the adiabatic representation. The QD states are dynamically updated for each nuclear propagation step, and remain to be a convenient and compact basis for quantum dynamics propagation. Further, the QD scheme provides a much more stable propagation compared to the adiabatic scheme as it does not explicitly require derivative couplings in the equation of motion. Because QD states are just the adiabatic states, they can be easily obtained from any routinely available electronic structure calculation. Thus, with many appealing features of SQC,<sup>1,6</sup> the QD-SQC approach developed in this work are promising for accurate and efficient *ab-initio* on-the-fly simulations in complex molecular systems.

## V. ACKNOWLEDGEMENT

This work was supported by the University of Rochester startup funds. Computing resources were provided by the Center for Integrated Research Computing (CIRC) at the University of Rochester. P.H. appreciates valuable discussions with Prof. Joe Subotnik and Prof. Artur Izmaylov.

## VI. APPENDIX A: MMST HAMILTONIAN IN THE ADIABATIC REPRESENTATION

Here we provide the detailed expression of the adiabatic MMST Hamiltonian. In the adiabatic representation, the total Hamiltonian in Eqn. 1 is expressed as the

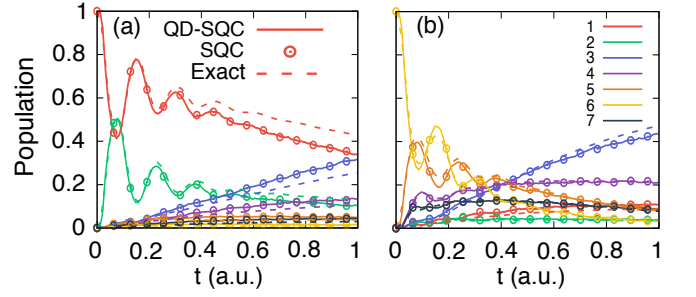


FIG. 7. Excitation energy transfer (EET) dynamics in a model Fenna-Matthews-Olson (FMO) complex. Diabatic state populations with an initial excitation on (a) state  $|1\rangle$  or (b) state  $|6\rangle$  are presented. Results are obtained from SQC (open circles), QD-SQC (solid lines), and numerical exact calculations (dash lines).

following “vibronic” Hamiltonian operator (with  $\hbar = 1$ )

$$\hat{H} = \frac{\hat{\mathbf{P}}^2}{2M} + \sum_i E_i(\mathbf{R}) |\Phi_i(\mathbf{r}; \mathbf{R})\rangle \langle \Phi_i(\mathbf{r}; \mathbf{R})| \quad (24)$$

$$- \sum_{ij} \left[ i \frac{\hat{\mathbf{P}}}{M} \mathbf{d}_{ij}(\mathbf{R}) + \frac{D_{ij}(\mathbf{R})}{2M} \right] |\Phi_i(\mathbf{r}; \mathbf{R})\rangle \langle \Phi_j(\mathbf{r}; \mathbf{R})|,$$

where  $\mathbf{d}_{ij}(\mathbf{R}) = \langle \Phi_i(\mathbf{r}; \mathbf{R}) | \nabla | \Phi_j(\mathbf{r}; \mathbf{R}) \rangle$  is the derivative coupling vector,  $D_{ij}(\mathbf{R}) = \langle \Phi_i(\mathbf{r}; \mathbf{R}) | \nabla^2 | \Phi_j(\mathbf{r}; \mathbf{R}) \rangle$  is the second-derivative coupling, and the diagonal terms  $D_{ii}(\mathbf{R})$  are usually referred as the Born-Oppenheimer (BO) corrections.

Note that this vibronic Hamiltonian in Eqn. 24 can also be written as<sup>17</sup>

$$\hat{H} = \sum_i E_i(\mathbf{R}) |\Phi_i(\mathbf{r}; \mathbf{R})\rangle \langle \Phi_i(\mathbf{r}; \mathbf{R})| \quad (25)$$

$$+ \sum_{ij} \frac{1}{2M} \left( \hat{\mathbf{P}} \delta_{ij} - i \hbar \mathbf{d}_{ij}(\mathbf{R}) \right)^2 |\Phi_i(\mathbf{r}; \mathbf{R})\rangle \langle \Phi_j(\mathbf{r}; \mathbf{R})|,$$

where the second-derivative coupling does not explicitly appear, but will indeed arise<sup>17</sup> through the noncommutativity between  $\hat{\mathbf{P}}$  and  $\mathbf{d}_{ij}(\mathbf{R})$ .

Applying mapping representation  $|\Psi_i(\mathbf{R})\rangle \langle \Psi_j(\mathbf{R})| \rightarrow \hat{a}_i^\dagger \hat{a}_j$  for the adiabatic states of the above vibronic Hamiltonian in Eqn. 25 leads to the standard adiabatic MMST Hamiltonian<sup>14,17</sup> as follows

$$\hat{H} = \frac{1}{2M} \left( \hat{\mathbf{P}} + \sum_{ij} \hat{q}_i \hat{p}_j \mathbf{d}_{ij}(\mathbf{R}) \right)^2 + \frac{1}{2} \sum_i E_i(\mathbf{R}) \left( \hat{q}_i^2 + \hat{p}_i^2 - 2\gamma \right), \quad (26)$$

where  $\gamma = 0.5$  is the ZPE of the mapping oscillator.

Replacing quantum mechanical operators with classical variables, we have the following classical Hamiltonian

$$H = \frac{1}{2M} (\mathbf{P} + \Delta \mathbf{P})^2 + \frac{1}{2} \sum_i E_i(\mathbf{R}) (q_i^2 + p_i^2 - 2\gamma), \quad (27)$$

where  $\Delta\mathbf{P}(\mathbf{R}, \mathbf{p}, \mathbf{q}) = \sum_{ij} q_i p_j \mathbf{d}_{ij}(\mathbf{R})$ . Classical equation of motion can thus be generated from the above Hamiltonian. However, it is computationally inconvenient, as the nuclear gradient explicitly depends upon the derivative of the derivative coupling,  $\nabla \mathbf{d}_{ij}(\mathbf{R}) = \partial \mathbf{d}_{ij}(\mathbf{R}) / \partial \mathbf{R}$ . Evaluating this term with electronic structure calculations is equivalent to compute the second derivative couplings, which remains extremely expensive. Thus, the MMST theory in the adiabatic representation significantly increases the complexity for quantum dynamics propagations.

## VII. APPENDIX B: KINEMATIC MOMENTUM TRANSFORMATION

In this section we briefly summarize the kinematic momentum (KM) transformation approach developed by Cotton and Miller,<sup>17</sup> which leads to an equivalent set of Hamilton's equations of motion (EOM) that do not explicitly contain  $\nabla \mathbf{d}_{ij}(\mathbf{R})$ . The *kinematic* momentum  $\tilde{\mathbf{P}}$  is obtained through the following transformation

$$\tilde{\mathbf{P}} = \mathbf{P} + \Delta\mathbf{P}. \quad (28)$$

With this new set of the canonical variables,  $\{\mathbf{R}, \tilde{\mathbf{P}}\}$ , one can generate an equivalent set of EOMs that do not explicitly contain  $\nabla \mathbf{d}_{ji}(\mathbf{R})$  as follows

$$\begin{aligned} \dot{q}_i &= \frac{\partial V_{\text{ad}}}{\partial p_i} + \sum_j q_j \mathbf{d}_{ji}(\mathbf{R}) \cdot \frac{\tilde{\mathbf{P}}}{M} \\ \dot{p}_i &= -\frac{\partial V_{\text{ad}}}{\partial q_i} + \sum_j p_j \mathbf{d}_{ji}(\mathbf{R}) \cdot \frac{\tilde{\mathbf{P}}}{M} \\ \dot{\mathbf{R}} &= \frac{\tilde{\mathbf{P}}}{M} \\ \dot{\tilde{\mathbf{P}}} &= -\frac{\partial V_{\text{ad}}}{\partial \mathbf{R}} + \sum_{ij} (\dot{q}_i p_j + q_i \dot{p}_j) \mathbf{d}_{ij}(\mathbf{R}). \end{aligned} \quad (29)$$

Here, the adiabatic potential is defined as  $V_{\text{ad}}(\mathbf{q}, \mathbf{p}, \mathbf{R}) = \frac{1}{2} \sum_i (p_i^2 + q_i^2 - 2\gamma) E_i(\mathbf{R})$ . On the other hand, the EOMs explicitly contain  $\mathbf{d}_{ji}(\mathbf{R})$ , which could lead to numerical instabilities when these derivative couplings are highly peaked.

## VIII. APPENDIX C: QD-SQC RESULTS FOR SPIN-BOSON SYSTEM

Here, we provide additional results of spin-boson model calculations with various electronic biases and temperatures, compared to the numerical exact results. Fig. 8 presents the population dynamics obtained from SQC, QD-SQC, and numerical exact quasi-adiabatic propagator path integral (QUAPI) calculations.<sup>47,48</sup> In all test cases, QD-SQC (solid lines) provides identical results compared to SQC (open circles), which are close to the exact QUAPI results (filled circles).

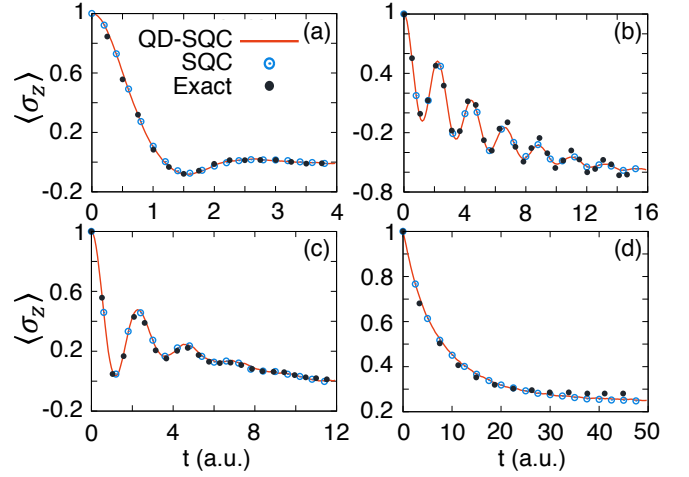


FIG. 8. Population dynamics of the spin-boson model with various bias  $\epsilon$  and temperature with (a)  $\epsilon = 0$ ,  $(k_B T)^{-1} = 0.1$ ,  $\xi = 0.09$  (b)  $\epsilon = 1$ ,  $(k_B T)^{-1} = 5$ ,  $\xi = 0.25$ , (c)  $\epsilon = 1$ ,  $(k_B T)^{-1} = 0.25$ ,  $\xi = 0.1$ , and (d)  $\epsilon = 5$ ,  $(k_B T)^{-1} = 0.1$ ,  $\xi = 0.4$ . Results are obtained from SQC (open circles), QD-SQC (solid lines), and numerical exact calculations (filled circles).

- <sup>1</sup>S. J. Cotton and W. H. Miller, J. Chem. Phys. **139**, 234112 (2013).
- <sup>2</sup>S. J. Cotton, K. Igumenshchev, and W. H. Miller, J. Chem. Phys. **141**, 084104 (2014).
- <sup>3</sup>W. H. Miller and S. J. Cotton, J. Chem. Theory Comput. **12**, 983 (2016).
- <sup>4</sup>S. J. Cotton and W. H. Miller, J. Chem. Phys. **145**, 144108 (2016).
- <sup>5</sup>G. Tao, J. Phys. Chem. C **118**, 17299 (2014).
- <sup>6</sup>W. H. Miller and S. J. Cotton, Faraday Discuss. **195**, 9 (2016).
- <sup>7</sup>W. H. Miller and S. J. Cotton, J. Chem. Phys. **142**, 131103 (2015).
- <sup>8</sup>N. Bellonzi, A. Jain, and J. E. Subotnik, J. Chem. Phys. **144**, 154110 (2016).
- <sup>9</sup>W. H. Miller and S. J. Cotton, J. Chem. Phys. **145**, 081101 (2016).
- <sup>10</sup>G. Tao, J. Phys. Chem. Lett. **7**, 4335 (2016).
- <sup>11</sup>G. Tao and N. Shen, J. Phys. Chem. A **121**, 1734 (2017), pMID: 28177246.
- <sup>12</sup>A. A. Kananenka, C.-Y. Hsieh, J. Cao, and E. Geva, J. Phys. Chem. Lett. **9**, 319 (2018), pMID: 29239614.
- <sup>13</sup>A. Jain and J. E. Subotnik, J. Phys. Chem. A **122**, 16 (2018).
- <sup>14</sup>N. Ananth, C. Venkataraman, and W. H. Miller, J. Chem. Phys. **127**, 084114 (2007).
- <sup>15</sup>P. Huo and D. F. Coker, J. Chem. Phys. **137**, 22A535 (2012).
- <sup>16</sup>C.-Y. Hsieh, J. Schofield, and R. Kapral, Mol. Phys. **111**, 3546 (2013).
- <sup>17</sup>S. J. Cotton, R. Liang, and W. H. Miller, J. Chem. Phys. **147**, 064112 (2017).
- <sup>18</sup>T. van Voorhis, T. Kowalczyk, B. Kaduk, L.-P. Wang, C.-L. Cheng, and Q. Wu, Annu. Rev. Phys. Chem. **61**, 149 (2010).
- <sup>19</sup>J. E. Subotnik, E. C. Alguire, Q. Ou, B. R. Landry, and S. Fatehi, Acc. Chem. Res. **48**, 1340 (2015).
- <sup>20</sup>A. Kubas, F. Hoffmann, A. Heck, H. Oberhofer, M. Elstner, and J. Blumberger, J. Chem. Phys. **140**, 104105 (2014).
- <sup>21</sup>X. Zeng, X. Hu, and W. Yang, J. Chem. Theory Comput. **8**, 4960 (2012).
- <sup>22</sup>A. Sirjoosingh and S. Hammes-Schiffer, J. Chem. Theory Comput. **7**, 2831 (2011).
- <sup>23</sup>A. Mandal, S. S. Yamijala, and P. Huo, J. Chem. Theory Comput. **14**, 1828 (2018).
- <sup>24</sup>H. Meyer and W. H. Miller, J. Chem. Phys. **70**, 3214 (1979).

- <sup>25</sup>G. Stock and M. Thoss, Phys. Rev. Lett. **78**, 578 (1997).
- <sup>26</sup>M. Thoss and G. Stock, Phys. Rev. A **59**, 64 (1999).
- <sup>27</sup>W. H. Miller, J. Phys. Chem. A **105**, 2942 (2001).
- <sup>28</sup>U. Müller and G. Stock, J. Chem. Phys. **111**, 77 (1999).
- <sup>29</sup>P. V. Parandekar and J. C. Tully, J. Chem. Theory Comput. **2**, 229 (2006).
- <sup>30</sup>C. A. Mead and D. G. Truhlar, J. Chem. Phys. **77**, 6090 (1982).
- <sup>31</sup>F. Webster, P.J.Rossky, and R.A.Friesner, Comput. Phys. Commun. **63**, 494 (1991).
- <sup>32</sup>G. A. Meek and B. G. Levine, J. Phys. Chem. Lett. **5**, 2351 (2014).
- <sup>33</sup>A. Jain, E. Alguire, and J. E. Subotnik, J. Chem. Theory Comput **12**, 5256 (2016).
- <sup>34</sup>S. Hammes-Schiffer and J. C. Tully, J. Chem. Phys. **12**, 4657 (1994).
- <sup>35</sup>N. Yu, C. Margulis, and D. Coker, J. Phys. Chem. B **105**, 6728 (2001).
- <sup>36</sup>G. Granucci, M. Persico, and A. Toniolo, J. Chem. Phys. **114**, 10608 (2001).
- <sup>37</sup>F. Plasser, G. Granucci, J. Pittner, M. Barbatti, M. Persico, and H. Lischka, J. Chem. Phys. **137**, 22A514 (2012).
- <sup>38</sup>G. A. Meek and B. G. Levine, J. Chem. Phys. **145**, 184103 (2016).
- <sup>39</sup>G. A. Meek and B. G. Levine, J. Chem. Phys. **145**, 184103 (2016).
- <sup>40</sup>D. V. Makhov, W. J. Glover, T. J. Martinez, and D. V. Shalashilin, J. Chem. Phys. **141**, 054110 (2014).
- <sup>41</sup>S. Fernandez-Alberti, D. V. Makhov, S. Tretiak, and D. V. Shalashilin, Phys. Chem. Chem. Phys. **18**, 10028 (2016).
- <sup>42</sup>L. Joubert-Doriol and A. F. Izmaylov, J. Chem. Phys. **148**, 114102 (2018).
- <sup>43</sup>N. Makri, J. Phys. Chem. B **103**, 2823 (1999).
- <sup>44</sup>A. Ishizaki and G. R. Fleming, Proc. Nat. Acad. Sci. U.S.A. **106**, 17255 (2009).
- <sup>45</sup>J. C. Tully, J. Chem. Phys. **93**, 1061 (1990).
- <sup>46</sup>G. Stock, J. Chem. Phys. **103**, 2888 (1995).
- <sup>47</sup>P. L. Walters and N. Makri, J. Chem. Phys. **144**, 044108 (2016).
- <sup>48</sup>D. E. Makarov and N. Makri, Chem. Phys. Lett. **221**, 482 (1994).